Received: 23 April 2019 | Revised: 2 August 2019 | Accepted: 18 September 2019

DOI: 10.1002/adc2.19

ORIGINAL ARTICLE

WILEY

Design and stability analysis of a super-twisting controller for a PS-FBC–based fuel cell module

Jorge L. Anderson Azzano | **Jerónimo J. Moré** | **Paul F. Puleston**

LEICI, Instituto de investigación en Electrónica, Control y Procesamiento de señales, Facultad de Ingeniería UNLP - CONICET, La Plata, Argentina

Correspondence
Jorge L. Anderson Azzano, LEICI, Instituto de investigación en Electrónica, Control y Procesamiento de señales, Facultad de Ingeniería UNLP - CONICET, Calle 48 y 116, CC 91, La Plata 1900, Argentina.
Email: anderson.jorgeluis@gmail.com

Funding information
Universidad Nacional de La Plata; Consejo Nacional de Investigaciones Científicas y Técnicas (CONICET); Agencia Nacional de Promoción Científica y Tecnológica (ANPCyT)

Abstract

Proton-exchange membrane fuel cells have been established as a really promising technology, specially due to their high efficiency and scalability features, additionally to their low pollution emissions. In a typical topology, fuel cell module (FCM) is usually integrated into a hybrid power system, where the FCM is designed to satisfy the main power requirements and reduce the current ripple at the fuel cell output. In this framework, the aim of this paper is to analyze and design a sliding mode control (SMC) for a FCM based on an isolated phase-shifted full bridge converter. This particular topology provides a high conversion ratio and attains a reduction of switching losses, which allow its application in low and medium power systems. From the control viewpoint, the proposed module represents a challenge due to the highly nonlinear behavior and wide operation range of the FCM, together with system parameter uncertainties and perturbations. To solve these issues, a second-order sliding mode super-twisting algorithm (STA) is proposed. As its main advantage, the STA reduces significantly the control chattering while preserving several features of conventional SMCs, such as robustness and finite time convergence. In order to analyze the zero dynamics stability, a Lyapunov study is proposed, taking advantage of its particular Liénard-type system structure. Finally, the designed algorithm is thoroughly analyzed and validated by computer simulation on a commercial 10-kW FCM and compared to first-order SMC.

KEYWORDS

hybrid power system, PEM fuel cell, super-twisting algorithm

1 | INTRODUCTION

In recent years, the increasing concern about global warming has focused the world's interest on alternative sources of energy. In the latest years, due to high efficiency, reliability, and clean energy, fuel cells (FCs) have awoken as a promising technology for reducing pollution emissions.

A hydrogen-based FC is an electrochemical device that produces electricity through the oxidation of hydrogen, with water and heat as byproducts. Different FCs exist depending on the electrolyte and the type of reaction involved. One of the most promising is the proton-exchange membrane fuel cell (PEM-FC), which has enhanced special interest for transportation applications[1] and has also been considered for power system generation and portable applications.[2,3] The main advantages of the PEM-FC are its low operating temperature, compactness, reduced weight, scalability, high efficiency, and high energy density. However, its high cost and relatively reduced lifetime remain as the main disadvantages of this FC technology.[4]

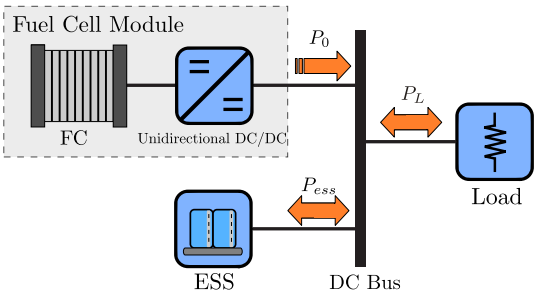

FIGURE 1 Schematic diagram of a fuel cell module as a part a hybrid power system. ESS, energy storage system; FC, fuel cell

From the electrical systems perspective, the FCs also present some drawbacks for their integration into a power system, mainly because of important nonlinearities and wide variations in their output voltage. In addition, due to a lack of bidirectional current flow, a slow dynamic response against load changes, and the already mentioned wide voltage variations, the FC needs to be integrated into a power conditioning system. Moreover, in order to satisfy the power demand of a changing load, it is indispensable to incorporate the FC system into a hybrid power system.

Diverse topologies of hybrid power systems that also involve an energy storage system (ESS) are described in the literature.[5-7] The auxiliary ESS is usually designed to provide peak-load demand and to regulate the voltage of a common DC bus. In this way, the FC is normally connected to the bus of the hybrid system through a DC/DC converter (see Figure 1). This converter must be able to operate efficiently under all FC module (FCM) conditions, while ensuring low ripple at the FC output current and increasing its useful life.

To fulfill such requirements, the family of converters known as isolated DC/DC converters presents interesting features to deal with hybrid power systems that involve FCMs. In view of the low output voltage of the FC, these converters provide a high conversion ratio through their high-frequency transformer (HFT). Furthermore, the recent developments in planar magnetic technology led to cost, size, and weight reduction, improving the performance of the overall system.[8,9] In particular, the phase-shifted full bridge converter (PS-FBC) diminishes switching stress, allowing its application in low and medium power systems.[10] In addition, the PS-FBC is capable of using zero-voltage switching techniques to attain a reduction of switching losses.[11]

In this context, the control system plays a fundamental role. On account of the inherent nonlinearities of the FC and its power conditioning system, linear control techniques usually have low performance,[12] which is worsened due to its wide range of operation. Moreover, the existence of uncertainties and disturbances demands the utilization of a robust controller capable of ensuring stability and performance for such operation range. In the past, very satisfactory results have been obtained using sliding mode control (SMC) for PS-FBCs,[13,14] but chattering effect remains as its main drawback.

Evolving from classic SMC, second-order sliding mode (SOSM) has emerged as a powerful approach to mitigate chattering issues, with innovative contributions that continues to this day.[15-19] This kind of algorithms preserves conventional SMC's features of robustness and finite-time convergence, while providing chattering reduction. The presented chattering amelioration allows reducing losses and increases the FCM lifetime. Therefore, in this work an SOSM super-twisting algorithm (STA) for a PS-FBC–based FCM is analyzed and developed. The STA controller allows its application directly to systems with relative degree one, as in the present topology, achieving a reduction of the chattering through its continuous control action. In addition, the proposed STA has low computational complexity for online applications.

On the other hand, it has been widely reported in the literature[20] that, when a power system is designed to control electrical power delivered to a constant DC bus, its internal dynamics could present stability issues. Regarding this problem, eigenvalue analysis is commonly performed in the literature[21-23] to the study of microgrid applications with constant input voltage sources. However, this linearized analysis could not be sufficient for systems that involve FCs due to their high nonlinearity and wide voltage variation. Therefore, it becomes necessary to establish a general condition that guarantee the secure operation of the FCM, in all its range. For this reason, a Lyapunov study is proposed in this paper to analyze the nonlinear internal dynamics of the FCM. This study is performed taking advantage of its particular Liénard-type system structure, establishing a sufficient condition to achieve the control system stability.

The structure of this paper is organize as follows. In Section 2, the electrical model of the PS-FBC–based FCM, employed in the control analysis, is described. The design procedure of the proposed SOSM-STA is presented and developed in Section 3. In Section 4, the zero dynamics (ZD) of the control system are analyzed by means of a Lyapunov approach, finding a sufficient condition to guarantee their stability. In Section 5, the designed algorithm is thoroughly analyzed and validated by computer simulation on a commercial 10-kW FCM and compared to first-order SMC. Finally, in Section 6, the conclusions and future works are discussed.

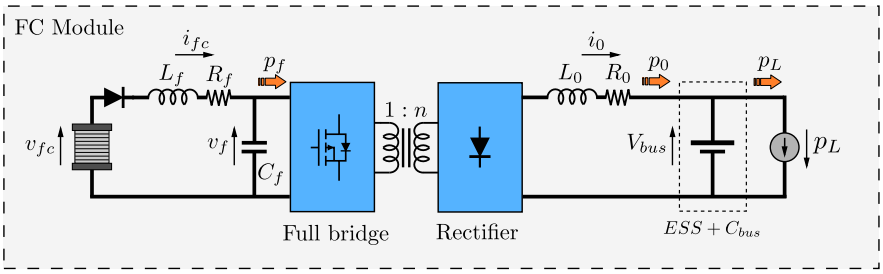

FIGURE 2 Phase-shifted full bridge converter–based fuel cell (FC) module

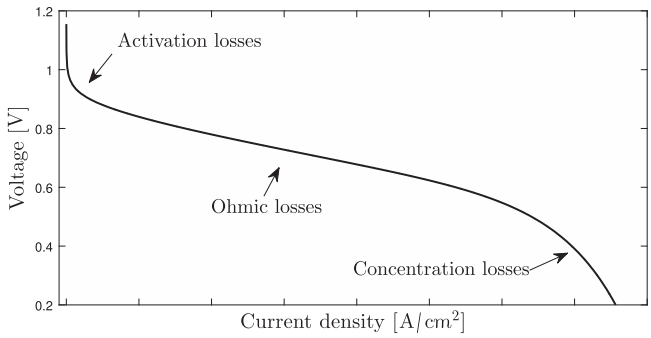

FIGURE 3 A typical voltage-current density curve of an individual proton-exchange membrane fuel cell

2 | MODELING OF THE FCM

The FCM under study is considered to operate as the core of a hybrid power system, where an auxiliary ESS assists the FCM to supply the peak-load power and to regulate the bus voltage of a common DC bus, as was shown in Figure 1. This system structure is capable of functioning over a wide operating range, satisfying abruptly variable electric loads like the ones present in electrical vehicles.

In this topology, the FC is connected to the DC link through a cascaded second-order filter and a dedicated DC/DC PS-FBC (see Figure 2). The FCM is responsible for managing the main power required by the variable load, while safeguarding the FC integrity and increasing its lifetime.

In the remainder of this section, the modeling of the PS-FBC–based FCM is described.

2.1 | PEM fuel cell

As was mentioned earlier, PEM-FC voltage is a nonlinear function of the power load, as well as the temperature and pressure of the FC. The output voltage of an individual cell V_{cell} can be described, by considering its three most relevant losses,[24]

$$V_{cell} = E - \Delta V_{act} - \Delta V_{ohm} - \Delta V_{conc},$$

where E is the theoretical open circuit voltage of a hydrogen FC, which highly depends on temperature and partial pressures. ΔV_{act}, ΔV_{ohm}, and ΔV_{conc} are the activation, ohmic, and concentration losses, respectively. Their effects are displayed in Figure 3 (for constant temperature and pressure).

At low current, there is a voltage drop due to the necessary energy to start the chemical reaction. These activation losses ΔV_{act} can be described by the Tafel equation. The ΔV_{ohm} are the losses due to electrical and ionic resistance of electrodes and electrolyte, resulting in a linear loss. Lastly, the ΔV_{conc} represents losses due to changes in reactant concentrations, which produce a reduction in their partial pressures. This voltage drop can be described empirically by an exponential law, leading to an important loss at high current.

Assuming regulated temperatures and partial pressures, an empirical model that provides a very good fit to experimental results of real FC stacks is[24]

$$v_{fc}(i_{fc}) = N_{stack}.E_{nl} - v_{act}(i_{fc}) - v_{conc}(i_{fc}) - R_{ohm}.i_{fc}, \quad (1)$$

where the overvoltage due to activation and concentration losses, v_{act} and v_{conc}, respectively, can be described as nonlinear functions of the FC current

$$v_{act}(i_{fc}) = N_{stack}.A_t.ln(i_{fc}), \tag{2}$$

$$v_{conc}(i_{fc}) = N_{stack}.m.exp(n.i_{fc}), \tag{3}$$

with N_{stack} being the number of cells, E_{nl} the open circuit voltage, A_t the slope of the Tafel equation, and m and n empirical coefficients. The stack resistance in the ohmic losses as the linear term is given by

$$R_{ohm} = N_{stack}.r_{ohm}, \tag{4}$$

with r_{ohm} being the resistance of a single cell. The electrical static model described in (1) has been successfully applied to the power system analysis that involves FCs, and it is extensively used in the literature.[25-27] For these reasons, the presented static model is used in the following study to design the proposed system controller. Then, in Section 5, the analysis is validated through an extended model that includes the double layer effect of FCs.

2.2 | Phase-shifted full bridge converter

The main characteristic of the PS-FBC is to use an intermediate AC stage to obtain a high conversion ratio through an HFT. This feature is fundamental for low-voltage input applications, avoiding the converter to operate with a large duty cycle. On account of its switch stress reduction and low switching losses, converters based on soft-switched modulation techniques, such as phase-shifted, are particularly well suited to operate in medium-power applications.

As shown in Figure 2, the PS-FBC consists of a single-phase, full bridge inverter connected to the primary winding of the HFT. Each inverter's leg generates a square-wave signal, working with a 50% duty cycle. As a result of the phase shift ϕ between both legs, a three-level signal is produced over the HFT.[11] The secondary winding of the transformer is connected to a diode rectifier, linked to the common DC bus by the inductor L_0.

In addition, a second-order low-pass filter is included between the FC and the PS-FBC to allow a reduced ripple current at the FC output.

Under the following assumptions:

- the HFT is ideal,
- only output and filter inductor losses are considered, neglecting switches and diode losses,
- the output current i_0 never reaches a zero value, and
- the bus voltage is perfectly regulated by the ESS to a constant value, equal to V_{bus},

the model of the FCM, presented in Figure 1, is[28]

$$\begin{cases} L_f.\frac{d\bar{i}_{fc}}{dt} = -\bar{i}_{fc}.R_f - \bar{v}_f + v_{fc(\bar{i}_{fc})} \\ C_f.\frac{d\bar{v}_f}{dt} = \bar{i}_{fc} - \bar{i}_0.n.u_{(t)} \\ L_0.\frac{d\bar{i}_0}{dt} = -\bar{i}_0.R_0 - V_{bus} + n.\bar{v}_f.u_{(t)}, \end{cases} \tag{5}$$

where the state $\bar{i}_{fc}$ is the average current in the FC, $\bar{v}_f$ is the voltage across the input filter capacitor, and $\bar{i}_0$ is the current delivered to the DC bus. Additionally, $u_{(t)} = \frac{\phi_{(t)}}{\pi}$ is the normalized phase shift or duty cycle, with $0 < u_{min} < u_{(t)} < 1$. The u_{min} parameter is chosen in order to limit the operating range of the PS-FBC, avoiding discontinuous conduction mode. The last assumption implies that the ESS and the bus capacitor are viewed by the FCM as a regulated voltage source (see Figure 2).

The system described by (5) is a control affine nonlinear system, ie, it can be rewritten as

$$\dot{x} = f_{(x)} + g_{(x)}.u_{(t)}, \tag{6}$$

where

$$x = [\, x_1 \;\; x_2 \;\; x_3 \,]' = [\, \bar{i}_{fc} \;\; \bar{v}_f \;\; \bar{i}_0 \,]' \tag{7}$$

and

$$f_{(x)} = \begin{bmatrix} -\frac{R_f}{L_f}.x_1 - \frac{1}{L_f}.x_2 + \frac{v_{fc(x_1)}}{L_f} \\ \frac{1}{C_f}.x_1 \\ -\frac{R_0}{L_0}.x_3 - \frac{V_{bus}}{L_0} \end{bmatrix}, \tag{8}$$

$$g_{(x)} = \begin{bmatrix} 0 \\ -\frac{n}{C_f}.x_3 \\ \frac{n}{L_0}.x_2 \end{bmatrix}. \tag{9}$$

3 | DESIGN OF THE SOSM CONTROLLER FOR THE FCM

In this section, the design of the second-order SMC-STA for the FCM is developed. The controller is intended to satisfy the tracking of a continuous FCM power reference p_{0r}, provided by an external supervisory control (the latter is not presented in this work.[29,30] This power reference is a smooth signal specifically designed to deliver the average load power, avoiding abrupt variations of the FC current. Thence, the control objective can be written, by means of the SMC theory, as

$$\sigma_{(x,t)} = V_{bus}.x_3 - p_{0r(t)}, \tag{10}$$

where σ is a smooth function, usually called the *sliding variable*. Therefore, the objective is accomplished when the control strategy steers and maintains the sliding variable σ and its first derivative $\dot{\sigma}$ to zero, ie, when the system reaches and remains on the *sliding manifold*

$$\mathcal{S} = \left\{ \forall x \subset \mathbb{R}^3 \, : \, \sigma_{(x,t)} = \dot{\sigma}_{(x,t)} = 0 \right\}. \tag{11}$$

Taking advantage of the control affine structure and the relative degree one of σ with respect to the control action u, the expression of $\dot{\sigma}$ and $\ddot{\sigma}$ can be easily obtained from (6)-(10) as

$$\dot{\sigma}_{(x,t)} = \Phi_{(x,t)} + \Gamma_{(x)}.u_{(t)} \tag{12}$$

$$\ddot{\sigma}_{(x,u,t)} = \varphi_{(x,u,t)} + \Gamma_{(x)}.\dot{u}_{(t)}, \tag{13}$$

with

$$\Phi_{(x,t)} = \frac{d\sigma_{(x,t)}}{dx}.f_{(x)} - \dot{p}_{0r(t)}, \tag{14}$$

$$\Gamma(x) = \frac{d\sigma_{(x,t)}}{dx}.g_{(x)}, \tag{15}$$

and

$$\varphi_{(x,u,t)} = \dot{\Phi}_{(x,t)} + \dot{\Gamma}_{(x)}.u_{(t)}. \tag{16}$$

The SOSM design procedure implies bounding functions φ and Γ of the second time derivative $\ddot{\sigma}$.[31]

3.1 | SOSM-STA with feedforward action

To track the desired power reference, a two-term controller is proposed. The first term is a direct feedforward action u_{ff}, which is designed to steer the system near to the desired operation region $\sigma_{(x,t)} = 0$, but it is not capable of dealing with uncertainties and disturbances. The second term is an SOSM-based control action, u_{st}, which provides robust convergence to the sliding manifold $\mathcal{S}$ in finite time. Therefore, the proposed control action u is written as

$$u_{(x,t)} = u_{ff(x,t)} + u_{st(x,t)}. \tag{17}$$

The feedforward action u_{ff} is obtained considering the nominal system (see Figure 2) with no uncertainties. It leads to

$$u_{ff(x,t)} = \frac{i_{0r(t)}.R_0 + V_{bus}}{n.x_2}, \tag{18}$$

where the FCM current reference is

$$i_{0r(t)} = \frac{p_{0r(t)}}{V_{bus}}. \tag{19}$$

Next, to design the SOSM term, u_{st}, it is necessary to include the effect of the feedforward u_{ff} into (12)-(13), by substituting the proposed control (17) into (12). It follows that $\dot{\sigma}$ can be rewritten as

$$\dot{\sigma}_{(x,t)} = \Phi'_{(x,t)} + \Gamma_{(x)}.u_{st(x,t)}, \tag{20}$$

with

$$\begin{aligned}\Phi'_{(x,t)} &= \Phi_{(x,t)} + \Gamma_{(x)}.u_{ff(x,t)} \\ &= -\frac{R_0}{L_0}.V_{bus}.(x_3 - i_{0r(t)}) - \dot{p}_{0r(t)},\end{aligned} \tag{21}$$

$$\Gamma_{(x)} = \frac{n}{L_0}.x_2.V_{bus}. \tag{22}$$

Similarly, $\ddot{\sigma}$ is rewritten as

$$\ddot{\sigma}_{(x,u,t)} = \varphi'_{(x,u,t)} + \Gamma_{(x)}.\dot{u}_{st(t)}, \tag{23}$$

where

$$\varphi'_{(x,u,t)} = \dot{\Phi}'_{(x,t)} + \dot{\Gamma}_{(x)}.u_{st(t)}. \tag{24}$$

Note that the above equation is quite similar to (13) and its derivation is omitted for brevity, but it can be straightforwardly computed from the FCM equations.

It can be demonstrated[32] that, if there exist positive constants C, K_m, and K_M such that

$$|\varphi'_{(x,u,t)}| \leq C \text{ and } 0 < K_m \leq \Gamma_{(x)} \leq K_M, \tag{25}$$

a robust control action u_{st} that leads and maintains the system trajectories onto S in finite time is given by the SOSM-STA (see Figure 4)

$$u_{st(x,t)} = -\lambda.|\sigma_{(x,t)}|^{1/2}.\text{sign}(\sigma_{(x,t)}) + \omega \tag{26}$$

$$\dot{\omega} = -\alpha.\text{sign}(\sigma_{(x,t)}). \tag{27}$$

To guarantee this finite robust convergence of the algorithm, the controller parameters α and λ must be chosen to satisfy

$$\alpha > \frac{C}{K_m} \tag{28}$$

$$\lambda^2 > \frac{2}{K_m^2}\frac{(K_m.\alpha + C)^2}{(K_m.\alpha - C)}. \tag{29}$$

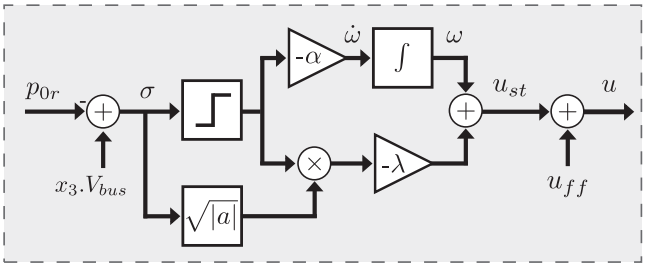

FIGURE 4 Scheme of the proposed control $u = u_{ff} + u_{st}$

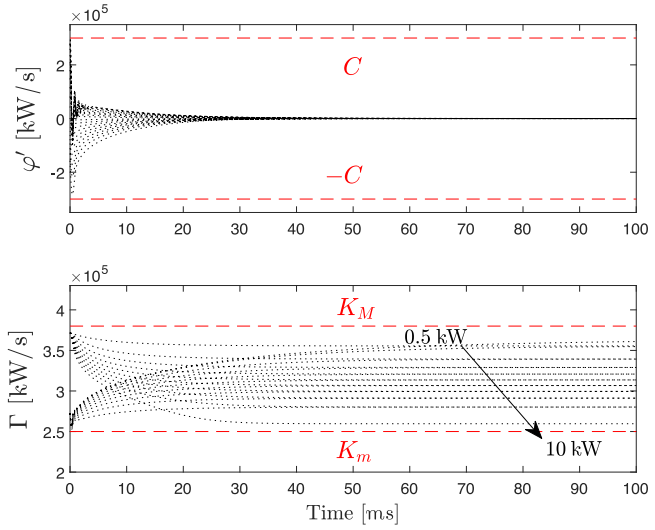

FIGURE 5 φ' and Γ functions evaluated for diverse system trajectories

The latter bounds are only a sufficient condition for the algorithm convergence and can be adjusted in order to improve the reduction of chattering.

3.2 | Bounding of φ' and Γ functions

From the bounds defined in (25), it is possible to find the controller parameters α and λ that ensure reaching the system trajectories onto S. In order to guarantee the control robustness, the positive constants C, K_m, and K_M must be computed considering the uncertainty of the system model and perturbations. For this work, a PS-FBC parameters variation of ±20% and a bus voltage variation of ±5% have been considered. Within those ranges of variations, the searched system bounds are basically defined by the worst-case combination of parameter uncertainties.

The expression of φ' can be obtained from (10)-(16), resulting in a quite complex equation. Bounding this expression analytically, usually, is an arduous procedure that leads to very conservative bounds. For this reason, in the present work, the constants C, K_m, and K_M have been obtained using a numerical approach.

To illustrate this numerical procedure, Figure 5 shows one of the sets of functions φ' and Γ that have been utilized for the practical tuning. The trajectories have been generated considering abrupt variations of u_{st}, which lead the system from the nominal power operation (∼10 kW) to a low power operation (∼0.5 kW), and vice versa.

After thorough simulation trials and analysis, where the system is evaluated taking into account the parameter variations previously mentioned, the desired bounds are determined. It should be noted that, in practice, even though numerically obtained, the controller parameters α and λ established by (28)-(29) should be iteratively adjusted in order to attain the desired robustness and chattering properties.

4 | LYAPUNOV ZERO DYNAMICS ANALYSIS BASED ON A LIÉNARD APPROACH

In addition to the reachability condition imposed by (28)-(29), the system dynamics over the sliding manifold S, ie, the ZD, should be analyzed to guarantee the control stability. In this way, it was identified that the particular ZD of the system can be reworked into a Liénard-type form.[33] This assists us to find a suitable energy-like Lyapunov function and, consequently, a stability condition for the FCM.

To this aim, the continuous control action u_{st}^{eq} required to maintain the system confined in the sliding surface S is obtained as[34]

$$u_{st(x,t)}^{eq} = -\frac{\Phi'_{(x,t)}}{\Gamma_{(x)}}\bigg|_{\sigma_{(x,t)}=0} = \frac{L_0}{n.V_{bus}}.\dot{p}_{0r(t)}.\frac{1}{x_2}. \tag{30}$$

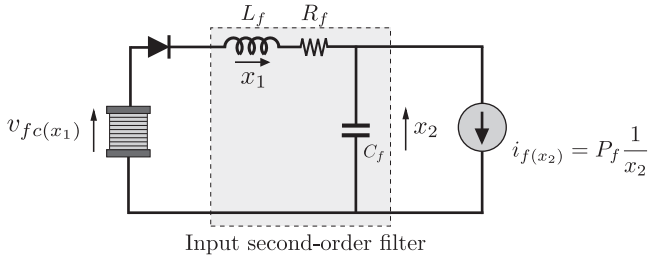

FIGURE 6 Equivalent electrical circuit of the zero dynamics

Hence, the ZD are computed by substituting the proposed control action (17) into the system equations (6)-(9), taking into account u_{st}^{eq} and the condition $\sigma_{(x,t)} = 0$. It follows that the ZD system results in

$$\begin{cases} L_f.\dot{x}_1 = -x_2 - R_f.x_1 + v_{fc(x_1)} \\ C_f.\dot{x}_2 = x_1 - p_{f(t)}\frac{1}{x_2}, \end{cases} \tag{31}$$

where $p_f(t) = R_0.i_{0r(t)}^2 + L_0.i_{0r(t)}.\dot{i}_{0r(t)} + p_{0r(t)}$ represents the instantaneous power at the FCM output.

As was previously stated, the variation of the external FCM power reference p_{0r} is in practice (see Section 5) much slower than the electrical response of the input filter (fast power variations are responsibility of the ESS, typically designed to provide peak load demand). Then, the first derivative of p_{0r} and of i_{0r} are negligible compared to the filter time constant thus, for the ZD analysis, the FCM power output p_f can be considered as

$$p_f(t) \approx R_0.I_{0r}^2 + P_{0r} = R_0.\frac{P_{0r}^2}{V_{bus}^2} + P_{0r} = P_f. \tag{32}$$

In this framework, the equivalent electrical circuit for the ZD is displayed in Figure 6.

The resulting electrical circuit presents stability issues, which have been extensively addressed in the literature for the particular case of a constant input voltage source.[22] These issues worsen in the studied case, because of the input voltage variations due to the FC as system source. Thus, it becomes necessary to go into an in-depth analysis to establish a comprehensive condition, which guarantees the system stability over a wide range of operation. To this aim, in the following study, a parameterization of the FC characteristic is developed, rewriting the FC voltage and its equivalent losses as functions of the different operation point throughout its range. Using a Taylor approach in the neighborhood of each one of these points, the parameterization gives

$$v_{fc}(x_1) = v_{fc}\left(x_1^0\right) + \left.\frac{\partial v_{fc}}{\partial x_1}\right|_{x_1^0}.\left(x_1 - x_1^0\right) + H.O.T. \tag{33}$$

$$\approx v_{fc}\left(x_1^0\right) + \left.\frac{\partial v_{fc}}{\partial x_1}\right|_{x_1^0}.\left(x_1 - x_1^0\right), \tag{34}$$

where x_1^0 is the equilibrium inductor current, for the admissible reference power values p_{0r}.

The above considerations lead to the following expression for the ZD:

$$\begin{cases} L_f.\dot{x}_1 = -x_2 - R\left(x_2^0\right).x_1 + V_{fc}\left(x_2^0\right) \\ C_f.\dot{x}_2 = x_1 - i_f(x_2), \end{cases} \tag{35}$$

where

$$R(x_2^0) = R_f - \left.\frac{\partial v_{fc}}{\partial x_1}\right|_{i_f(x_2^0)} \tag{36}$$

and

$$V_{fc}\left(x_2^0\right) = v_{fc}\left(i_f\left(x_2^0\right)\right) - \left.\frac{\partial v_{fc}}{\partial x_1}\right|_{i_f(x_2^0)}.i_f\left(x_2^0\right), \tag{37}$$

with

$$i_f(x_2) = P_f \frac{1}{x_2}. \tag{38}$$

As it can be seen, the parameterized losses $R(x_2^0)$ and FC voltage $V_{fc}(x_2^0)$ need to be computed for each operation point, defined by the reference power p_{0r}. This parameterization will help to find a valid condition for the nonlinear FC operation range. The equilibrium point determined by the current x_1^0 and voltage x_2^0, corresponding to the state variables x_1 and x_2, respectively, are obtained by

$$x_1^0 = i_f\left(x_2^0\right), \tag{39}$$

with x_2^0 a solution of the equation

$$v_{fc}\left(i_f\left(x_2^0\right)\right) = R_f.i_f\left(x_2^0\right) + x_2^0. \tag{40}$$

The dynamic system (35) has two equilibrium points, but just the equilibrium voltage x_2^0, which is closer to the FC voltage, has physical meaning and is considered in the analysis. The system states can be redefined shifting the equilibrium point to the origin as

$$\bar{x}_1 = x_1 - i_f\left(x_2^0\right) \tag{41}$$

$$\bar{x}_2 = x_2 - x_2^0, \tag{42}$$

leading to the transformed system form

$$\begin{cases} \dot{\bar{x}}_1 = -\frac{R(x_2^0)}{L_f}\bar{x}_1 - \frac{1}{L_f}\bar{x}_2 \\ \dot{\bar{x}}_2 = \frac{\bar{x}_1}{C_f} - \frac{1}{C_f}\left\{i_f\left(\bar{x}_2 + x_2^0\right) - i_f\left(x_2^0\right)\right\}. \end{cases} \tag{43}$$

Finally, applying the linear transformation

$$z_1 = \frac{1}{C_f}\bar{x}_1 + \frac{R\left(x_2^0\right)}{L_f}\bar{x}_2 \tag{44}$$

$$z_2 = \bar{x}_2, \tag{45}$$

we obtain the Liénard-type system

$$\dot{z}_1 = -g(z_2) \tag{46}$$

$$\dot{z}_2 = z_1 - F(z_2), \tag{47}$$

where

$$F(z_2) = \frac{R\left(x_2^0\right)}{L_f}.z_2 + \frac{1}{C_f}.\left\{i_f\left(z_2 + x_2^0\right) - i_f\left(x_2^0\right)\right\} \tag{48}$$

$$g(z_2) = \frac{1}{L_f C_f}.z_2 + \frac{R\left(x_2^0\right)}{L_f C_f}\left\{i_f\left(z_2 + x_2^0\right) - i_f\left(x_2^0\right)\right\}. \tag{49}$$

Due to the above functions that satisfy $g(0) = F(0) = 0$, the energy-like Lyapunov function of the transformed states z_1 and z_2

$$V(z_1, z_2) = \frac{1}{2}.z_1^2 + \mathcal{G}(z_2), \text{ with } \mathcal{G}(z_2) = \int_0^{z_2} g(\xi)d\xi \tag{50}$$

is locally positive-definite if $g(z_2)$ satisfies the following condition:

$$z_2.g(z_2) > 0, \tag{51}$$

for some interval

$$\mathcal{Z} = \{z_2 \in R - \{0\} : \underline{z_2} < z < \overline{z_2}; \quad \underline{z_2} < 0, \overline{z_2} > 0\}. \tag{52}$$

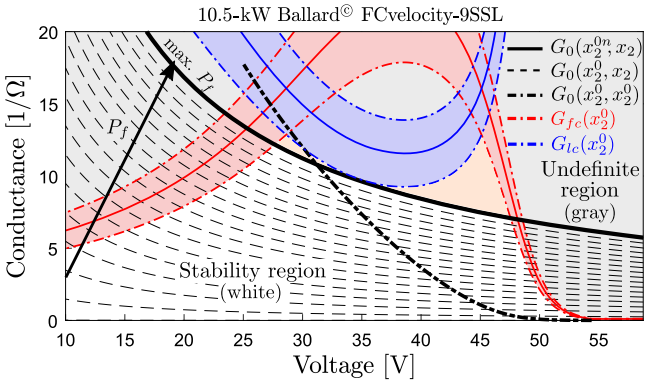

FIGURE 7 Conductance diagram of the 10.5-kW Ballard© fuel cell proposed to analyze the ZD stability

The first derivative of V is equal to

$$\dot{V}(z_1, z_2) = -g(z_2).F(z_2), \tag{53}$$

which is locally negative-definite if $g(z_2)F(z_2) > 0$.

Moreover, if condition (51) is satisfied, it follows that

$$\begin{aligned} g(z_2).F(z_2) > 0 \Rightarrow g(z_2)^2.z_2.F(z_2) > 0 \\ \Longleftrightarrow z_2.F(z_2) > 0. \end{aligned} \tag{54}$$

From Equations (48)-(49) and conditions (51) and (54), it can be easily shown that a sufficient condition for the local system stability, as function of the original state variable x_2, is determined by

$$G_0\left(x_2^0, x_2\right) < \min\left\{G_{fc}\left(x_2^0\right), G_{lc}\left(x_2^0\right)\right\}, \tag{55}$$

where the output conductance G_0 is equal to

$$G_0\left(x_2^0, x_2\right) = \frac{i_f(x_2) - i_f\left(x_2^0\right)}{x_2^0 - x_2}, \tag{56}$$

and the FC conductance G_{fc} and the filter conductance G_{lc}, respectively, are

$$G_{fc}\left(x_2^0\right) = \frac{1}{R\left(x_2^0\right)} \quad \text{and} \quad G_{lc}\left(x_2^0\right) = \frac{C_f}{L_f} R\left(x_2^0\right). \tag{57}$$

The local stability condition (55) makes possible to construct a conductance diagram as function of the capacitor voltage x_2, taking into account different operation points (ie, different values of P_f). Figure 7 shows a graphical representation of this condition, establishing a stability region (white area) where the ZD stability is locally guaranteed.

The stability region is delimited by the FC G_{fc} and the filter G_{lc} conductances. To contemplate parameter variations and modeling errors, safe bounds of 20% has been considered for both G_{lc} and G_{fc} (the corresponding curves are depicted in red and blue, respectively, in Figure 7). In this way, the output conductance at steady state, $G_0(x_2^0, x_2^0)$, remains inside this region, setting a secured voltage range for the filter capacitor.

5 | SIMULATION RESULTS

In this section, the performance of the designed SOSM-STA controller is assessed on a 10-kW FCM. To evaluate the robustness of the proposed method under realistic operating conditions, a higher-order model of the hybrid power system is used for the simulations (see Figure 8), incorporating system model disturbances, uncertainties and dynamics unmodeled during the design procedures. For the latter, the double layer phenomenon of FCs is taken into consideration for the simulation model,[35] through the insertion of the capacitor C_{dl} connected in parallel with activation and concentration losses. In addition, a dynamic model for the ESS was assumed, comprising supercapacitors and a typical PI controlled boost converter (see Appendix A).

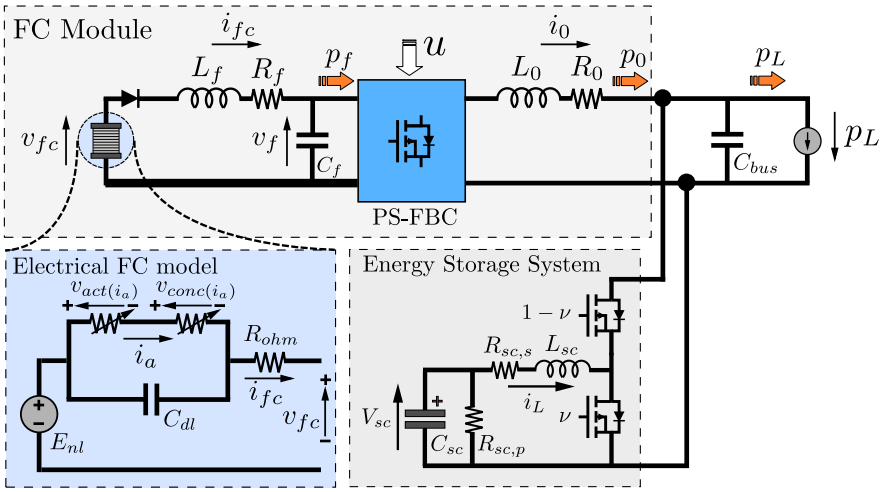

FIGURE 8 Electrical model of the hybrid power system employed in the fuel cell module validation. FC, fuel cell; PS-FBC, phase-shifted full bridge converter

TABLE 1 Parameters of the simulated 10-kW fuel cell module

PS-FBC parameters				FC parameters			
L_f	6 µH	R_0	100 mΩ	N_{stack}	55	E_{nl}	0.95 V
C_f	1550 µF	n	20	r_{ohm}	0.5 mΩ	A_t	45.56 mV
R_f	5 mΩ	V_{bus}	400 V	m	2 mV	n	$0.008\frac{1}{A}$
L_0	1000 µH	f_s	30 kHz	C_{dl}	4.9 F		
STA parameters				**ESS parameters**[37]			
α	0.14	C	$3.00e^5$ kW/s	V_{sc}^n	48 V	$R_{sc,s}$	10 mΩ
λ	$4.8e^{-4}$	K_m	$2.50e^5$ kW/s	C_{sc}	83 F	$R_{sc,p}$	16 kΩ
		K_M	$3.75e^5$ kW/s	L_{sc}	30 µH	C_{bus}	500 µF

Abbreviations: ESS, energy storage system; FC, fuel cell; PS-FBC, phase-shifted full bridge converter; STA, super-twisting algorithm.

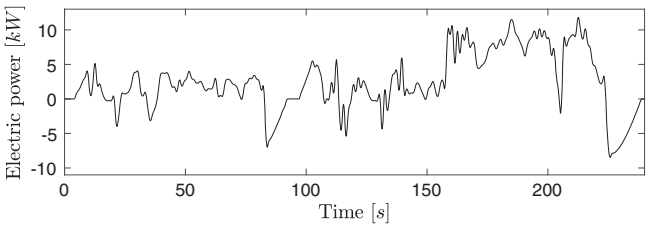

FIGURE 9 Load power profile p_L generated from the EPA IM240 driving urban cycle

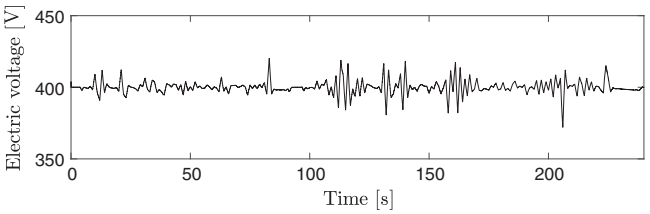

FIGURE 10 Time response of the perturbed bus voltage v_{bus}

The modeled FC is a *Ballard FCvelocity-9SSL* with a rated power of 10.5 kW. Equation (1) has been fitted to the FC polarization curve,[36] considering a nominal DC voltage of 35 V at 300 A. The HPS parameters employed in the simulations are presented in Table 1. The Table also presents the controller parameters obtained through the procedure described in Section 3.2. As was explained there, up to 20% system parameters uncertainties have been considered for the controller design. To assess the control system under adverse conditions, the following simulations have been conducted assuming the worst-case scenario regarding parameters uncertainties.

To evaluate the FCM control, the HPS is assumed to operate under highly variable power demand p_L. The power profile was generated in accordance with the EPA IM240 driving urban cycle, considering a 400-kg electric vehicle (see Figure 9). Additionally, the poorly regulated bus voltage v_{bus} is shown in Figure 10. As previously stated, to test the robustness of the SOSM-STA controller, voltage disturbances of 5% have been allowed.

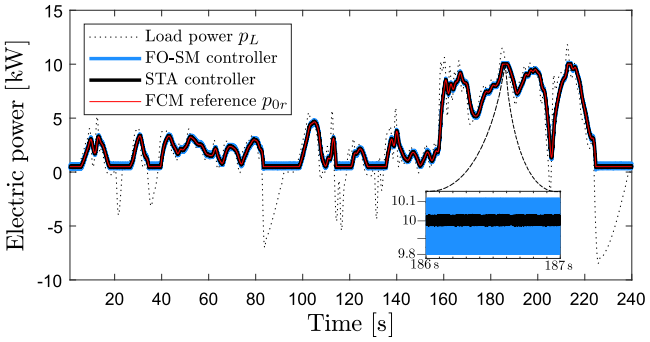

FIGURE 11 Control system tracking of the FCM power reference p_{0r}. FCM, fuel cell module; FO-SM, first-order sliding mode; STA, super-twisting algorithm

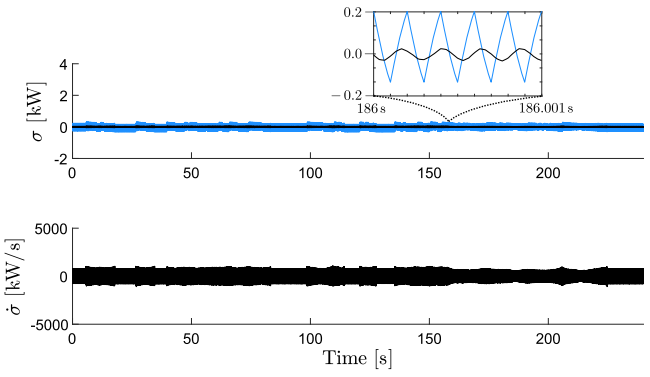

FIGURE 12 Time response of sliding variable σ and $\dot{\sigma}$

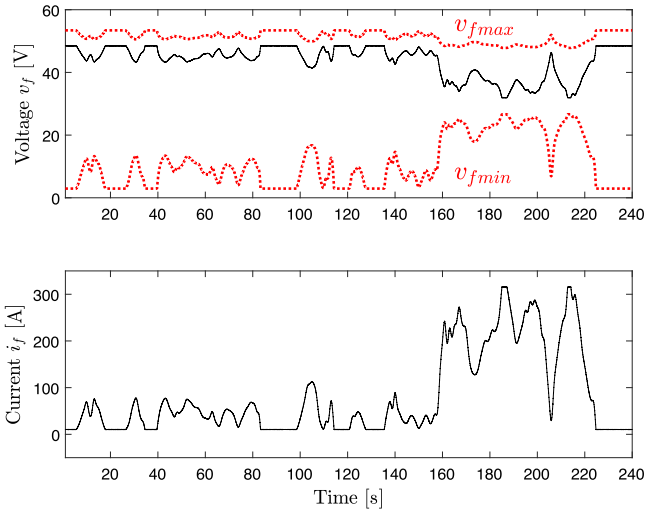

FIGURE 13 Stable response of zero dynamics states v_f and i_f

To safeguard the FC lifetime, the smooth FCM power reference p_{0r} was generated by means of a typical frequency decouple strategy,[30] with a cut-off frequency of 0.1 Hz (see Figure 11). Note that, as it was explained, the difference between load power p_L and FCM output power p_0 is provided by the ESS.

Figure 11 presents time response of designed SOSM-STA control system. In addition to the proposed controller, a conventional first-order SMC (FO-SMC) is also shown to compare their performance. The FO-SMC is designed in accordance to the system perturbation and uncertainties considered for the STA analysis (see Appendix B).

As it can be appreciated, both controllers achieve robust tracking for the FCM power output, p_{0r}, in spite of variable power demand, disturbed v_{bus}, and system uncertainties. Nevertheless, the STA achieves a considerable amelioration

of chattering, leading to an important control effort reduction. For illustrative purposes, the zoom in the Figure portrays the chattering of the proposed controller in the neighborhood of the nominal power, showing that it is lowered to approximately 25% of the FO-SMC chattering. In addition, a reduction of p_0 chattering basically results in lesser current chattering through the FCM and, consequently, power losses diminution, so overall efficiency is enlarged.

The evolution of σ and $\dot{\sigma}$ is presented in Figure 12, when the system has already reached the sliding manifold $\mathcal{S}$. It can be observed that, once the system is led onto $\mathcal{S}$ by the proposed SOSM-STA controller, it never leaves the sliding manifold, ensuring its robust permanency and, therefore, guaranteeing the tracking of the power reference p_{0r}. The detail shows the smooth variation of the STA that is responsible of the chattering reduction, with respect to the conventional SMC.

Figure 13 shows the stable response of the ZD states, v_f and i_f. As it can be appreciated, the stability region, computed by the analysis described in Section 4, settles upper and lower bounds for the voltage variations of the input filter. Inside this stable region, which is defined through the proper selection of the filter elements, the secure operation of the FC is guaranteed and the desired performance of the overall control system is assured.

6 | CONCLUSION

This paper proposed a power tracking SM controller for a PS-FBC–based FCM. This PS-FBC–based topology provides high conversion ratio through its HFT, which is required to deal with the low output voltage of the FC. This feature prevents the converter from operating with a large duty cycle and reduces system losses, allowing its application in medium power systems.

To reduce output chattering, typical in several SMC systems, a continuous SOSM controller based on a STA was developed. The proposed controller proves to successfully attain robust tracking of the power reference, in spite of variable power demand, voltage bus variations, and system parameters uncertainties.

To guarantee the stability of the controlled system on the sliding manifold $\mathcal{S}$, the ZD were analyzed. Due to ZD structure, standard Lyapunov functions were not applicable. To overcome this drawback, a diffeomorphism was used to bring the dynamics into a Liénard-type form, allowing the utilization of a special integral Lyapunov function.

Finally, it can be remarked that the designed super-twisting controller has low computational complexity, a very important feature for implementation. Additionally, the resulting FCM is highly versatile, ie, it is not restricted to a particular hybrid systems, but instead, it is feasible to be integrated into different topologies composed of diverse alternative sources/storage devices.

The forthcoming phase of this project is twofold. On the one hand, efforts will be focused on experimentally validating the satisfactory simulation results in an actual FC-based hybrid testbench. On the other, theoretical development will be undertaken to improve the proposed super twisting controller, particularly aiming to design an adaptive gain STA setups capable to further reduce the control effort and chattering.

ACKNOWLEDGEMENTS

This research was supported by the Universidad Nacional de La Plata, the Consejo Nacional de Investigaciones Científicas y Técnicas (CONICET), and the Agencia Nacional de Promoción Científica y Tecnológica (ANPCyT) from Argentina.

ORCID

Jorge L. Anderson Azzano https://orcid.org/0000-0003-4858-5442
Jerónimo J. Moré https://orcid.org/0000-0002-0700-2530

REFERENCES

1. Lai J-S, Ellis MW. Fuel cell power systems and applications. *Proc IEEE*. 2017;105(11):2166-2190.
2. Patterson M, Macia NF, Kannan AM. Hybrid microgrid model based on solar photovoltaic battery fuel cell system for intermittent load applications. *IEEE Trans Energy Convers*. 2015;30(1):359-366.
3. Tran V-L, Tran N-T, Yu S-H, Park Y, Choi W. Design of a nonisolated fuel cell boost charger for lithium polymer batteries with a low output ripple. *IEEE Trans Energy Convers*. 2015;30(2):605-614.

4. Wang Y, Chen KS, Mishler J, Chan Cho S, Cordobes Adroher X. A review of polymer electrolyte membrane fuel cell: Technology, applications, and needs on fundamental research. *Applied Energy*. 2011;88(4):981-1007.
5. Thounthong P, Rael S, Davat B. Analysis of supercapacitor as second source based on fuel cell power generation. *IEEE Trans Energy Convers*. 2009;24(1):247-255.
6. Hajizadeh A, Golkar MA, Feliachi A. Voltage control and active power management of hybrid fuel-cell/energy-storage power conversion system under unbalanced voltage sag conditions. *IEEE Trans Energy Convers*. 2010;25(4):1195-1208.
7. Abkenar AT, Nazari A, Jayasinghe SDG, Kapoor A, Negnevitsky M. Fuel cell power management using genetic expression programming in all-electric ships. *IEEE Trans Energy Convers*. 2017;32(2):779-787.
8. Ouyang Z, Andersen MAE. Overview of planar magnetic technology - fundamental properties. *IEEE Trans Energy Convers*. 2014;29(9):4888-4900.
9. Magambo JSNT, Bakri R, Margueron X, et al. Planar magnetic components in more electric aircraft: review of technology and key parameters for DC-DC power electronic converter. *IEEE Trans Transp Electrification*. 2017;3(4):831-842.
10. Kolli A, Gaillarda A, De Bernardinisb A, Bethouxc O, Hissela D, Khatir Z. A review on DC/DC converter architectures for power fuel cell applications. *Energy Convers Manag*. 2015;105:716-730.
11. Xinbo R. *Soft-Switching PWM Full-Bridge Converters: Topologies, Control and Design*. Singapore: Wiley; 2014.
12. Kunusch C, Puleston P, Mayosky M. *Sliding-Mode Control of PEM Fuel Cells*. London, UK: Springer; 2012.
13. Shams-Ansari A, Razavi F, Ghadimi A, Abolmasoumi H. Implementation of sliding mode control in a full bridge (DC-DC) converter. *Indian J Sci Technol*. 2012;5:2665-2672.
14. Senapati RN, Sahoo RK, Senapati R. Design and analysis of sliding mode controller for isolated full bridge DC-DC converter. Paper presented at: 1st IEEE International Conference on Power Electronics Intelligent Control and Energy Systems (ICPEICES-2016); 2016; Delhi, India.
15. Fridman L, Moreno J, Bandyopadhyay B, Kamal S, Chalanga A. *Continuous nested algorithms: the fifth generation of sliding mode controllers*. In: Recent Advances in Sliding Modes: From Control to Intelligent Mechatronics. Cham, Switzerland: Springer International Publishing; 2015.
16. Fridman L, Moreno J, Iriarte R. *Sliding Modes After the First Decade of the 21st Century*. Berlin, Germany: Springer; 2011.
17. Bandyopadhyay B, Sivaramakrishnan J, Spurgeon S. *Advances in Sliding Mode Control. Concept, Theory and Implementation*. Vol. 440. Berlin, Germany: Springer; 2013.
18. Fridman L, Barbot JP, Plestan F. *Recent Trends in Sliding Mode Control*. London, UK: IET; 2016.
19. Li S, Yu X, Fridman L, Man Z, Wang X. *Advances in Variable Structure Systems and Sliding Mode Control—Theory and Applications*. Vol. 115. Cham, Switzerland: Springer; 2018.
20. Singh S, Gautam A, Fulwani D. Constant power loads and their effects in DC distributed power systems: a review. *Renew Sustain Energy Rev*. 2017;72:407-421.
21. Alexey S, Machado JE, Ortega R, Schiffer J, Pyrkin AA. On the Existence and Long-Term Stability of Voltage Equilibria in Power Systems with Constant Power Loads. *CoRR*. 2018. abs/1809.08127
22. Liu J, Zhang W, Rizzoni G. Robust stability analysis of DC microgrids with constant power loads. *IEEE Trans Power Syst*. 2018;33(1):851-860.
23. Wu J, Lu Y. Adaptive backstepping sliding mode control for boost converter with constant power load. *IEEE Access*. 2019;7:50797-50807.
24. Larminie J, Dicks A. *Fuel Cell Systems Explained*. 2nd ed. Chichester, UK: Wiley; 2003.
25. Benmouna A, Becherif M, Depernet D, Ebrahim MA. Novel energy management technique for hybrid electric vehicle via interconnection and damping assignment passivity based control. *Renewable Energy*. 2018;119:116-128.
26. Kraa O, Ghodbane H, Saadi R, et al. Energy management of fuel cell/supercapacitor hybrid source based on linear and sliding mode control. *Energy Procedia*. 2015;74:1258-1264. Part of special issue: The International Conference on Technologies and Materials for Renewable Energy, Environment and Sustainability-TMREES15.
27. Moré J, Puleston P, Kunusch C, Fossas E. Multi input sliding mode control of an autonomous fuel cell-supercapacitor hybrid system. Paper presented at: 12th IEEE Workshop on Variable Structure Systems; 2012; Mumbai, India.
28. Ghadimi AA, Rastegar H, Keyhani A. Development of average model for control of a full bridge PWM DC-DC converter. *J Iran Assoc Electr Electron Eng*. 2007;4:52-59.
29. Moré JJ, Puleston PF, Kunusch C, Fantova MA. Development and implementation of a supervisor strategy and sliding mode control setup for fuel-cell-based hybrid generation systems. *IEEE Trans Energy Convers*. 2015;30(1):218-225.
30. Snoussi J, Benelghali S, Benbouzid M, Mimouni M. Optimal sizing of energy storage systems using frequency-separation-based energy management for fuel cell hybrid electric vehicles. *IEEE Trans Veh Technol*. 2018;67:9337-9346.
31. Levant A. Principles of 2-sliding mode design. *Automatica*. 2007;43(4):576-586.
32. Shtessel Y, Edwards C, Fridman L, Levant A. *Sliding Mode Control and Observation*. New York, NY: Springer; 2014.
33. Miyagi H, Munda JL, Miyagi N. Study on Lyapunov functions for Liénard-type nonlinear systems. *IEEE J Trans Electron Inf Syst*. 2001;121(4):748-755.
34. Utkin V. *Sliding Modes in Control and Optimization*. Berlin, Germany: Springer; 1992.
35. San Martin I, Ursúa A, Sanchis P. Modelling of PEM fuel cell performance: steady-state and dynamic experimental validation. *Energies*. 2014;7:670-700.

36. Ballard Power System, Inc. FCvelocity - 9SSL-Ballard Power. Technical report. Ballard. 2011. http://www.ballard.com
37. Maxwell Technologies, Inc. Datasheet - 48V Modules. Technical Report 1009365.13. 2013. https://www.maxwell.com/

How to cite this article: Anderson Azzano JL, Moré JJ, Puleston PF. Design and stability analysis of a super-twisting controller for a PS-FBC–based fuel cell module. *Adv Control Appl*. 2019;1:e19. https://doi.org/10.1002/adc2.19

APPENDIX A

SUPERCAPACITOR-BASED ESS MODULE

The control parameters of the ESS module, employed in the simulation results, are detailed in Table A1. To regulate the bus voltage, a typical nested PI controller setup applied to a boost converter (see Figure A1) was taken into account, achieving an overshoot of less than 5% and a settling time of 10 ms at nominal conditions.

TABLE A1 Control parameters of the energy storage system

External loop		Internal loop	
Ki_v	9.86	Ki_i	1.29
Kp_v	0.326	Kp_i	$0.452e^{-3}$

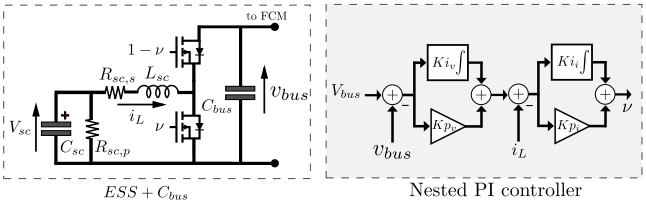

FIGURE A1 Schematic diagram of the energy storage system (ESS) topology and controller based on a nested proportional-integral (PI) controller

APPENDIX B

FIRST-ORDER SLIDING MODE CONTROLLER

In order to reduce control chattering and achieve a valid comparison for the proposed SOSM-STA controller, a two-term controller based on conventional SMC is designed, as well as in (17), ie,

$$u_{(x,t)} = u_{ff(x,t)} + u_{smc(x,t)}, \tag{B1}$$

where u_{ff} is equal to (18) and u_{smc} is a conventional SMC equals to

$$u_{smc(x,t)} = -k.\text{sign}(\sigma_{(x,t)}), \quad \text{with } k = 0.015. \tag{B2}$$